Macromolecules

pubs.acs.org/Macromolecules Article

# Permeability of Polymer Membranes beyond Linear Response

Won Kyu Kim,* Sebastian Milster, Rafael Roa, Matej Kanduč, and Joachim Dzubiella*

Cite This: https://doi.org/10.1021/acs.macromol.2c00605 Read Online

ACCESS | Metrics & More | Article Recommendations | Supporting Information

**ABSTRACT:** The permeability of a membrane to solute penetrants is well defined on the linear response level simply as the ratio of penetrants' flux and concentration gradient at the membrane boundary layers. However, nonlinearities emerge in the flux–force relation $j(f)$ for large driving forces $f$, in which the definition of permeability becomes ambiguous. Here, we study nonequilibrium membrane permeation orchestrated by a generic driving force using penetrant- and monomer-resolved computer simulations of transport in a polymer network, supported by exact solutions of the Smoluchowski (drift–diffusion) equation in the stationary state. In the simulations, we consider the transport across a finite polymer membrane immersed in a reservoir of penetrants, addressing one- and two-component penetrant systems. We calculate the $f$-dependent inhomogeneous steady-state density profiles, boundary layer concentrations, and fluxes of the penetrants. The Smoluchowski approach, using solely coarse-grained equilibrium partitioning and diffusion profiles as input, exhibits remarkable qualitative agreement with our nonequilibrium simulations, which serves for rationalization of the observations. We discuss possible definitions of nonequilibrium, $f$-dependent permeability, distinguishing between "system" and "membrane" permeabilities. In particular, we introduce the concept of *differential permeability* as a response to $f$. The latter turns out to be a highly *nonmonotonic* function of $f$ for low-permeable systems, demonstrating how a differential permselectivity is substantially tunable by the driving force beyond linear response.

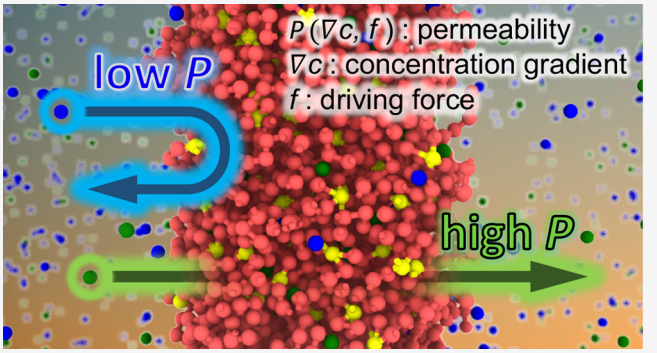




## INTRODUCTION

The permeability of polymeric membranes is a key functional property in biology and modern applications utilizing soft materials. Examples of polymer networks important for selective transport in living systems are cytoskeletons, mucus, and extracellular matrices.[1−7] Synthetic polymer networks, on the other hand, serve as indispensable building blocks in dialysis, nanofiltration and desalination,[8] drug delivery systems[9−11] or stimuli-responsive nanoreactors with applications in controllable nanocatalysis,[12−24] and biomedical diagnoses.[15−19] The transport embraces nanoscale atoms to sub-micron-scale macromolecules, such as ions, ligands, proteins, and reactants, which we refer to as "penetrants" of the membrane in the following. Particularly important for applications is to utilize solute selectivity in the permeability ("permselectivity"), as prominently found in air filtration or gas separation[25−34] and water purification.[35−42]

In its most basic and widely accepted definition, permeability ($\mathcal{P}$) is defined within the linear response regime, essentially as the ratio between the flux ($j$) and concentration gradient.[43−50] For this, consider the simple membrane model as illustrated in Figure 1(a) and Fick's type of permeation as illustrated in Figure 1(b). Here, the membrane permeability is defined as the proportionality constant of the flux,

$$j \equiv -\mathcal{P}\frac{\Delta c_0}{d} \tag{1}$$

driven by the penetrant concentration difference $\Delta c_0 = c_{0R} - c_{0L}$ between both reservoir sides of the membrane of thickness $d$. In this work, we consider the number concentration (i.e., the penetrant number divided by the volume). Based on the standard constitutive transport equations for dense membranes, which leads to the well-known solution–diffusion model,[25,26,44−59] the linear response permeability can be written as

$$\mathcal{P} = D_{in}\mathcal{K} \tag{2}$$

which is the trade-off relation between the two key quantities, $\mathcal{K}$ and $D_{in}$. [In this work, we consider $\mathcal{P} = D_{in}\mathcal{K}$, which is independent of the membrane thickness $d$. Some works use a different definition, $\mathcal{P} = D_{in}\mathcal{K}/d$.] The former is the partition coefficient (or the partition ratio) $\mathcal{K} \equiv c_{in}/c_0$, that is, the ratio

Received: March 24, 2022
Revised: May 29, 2022

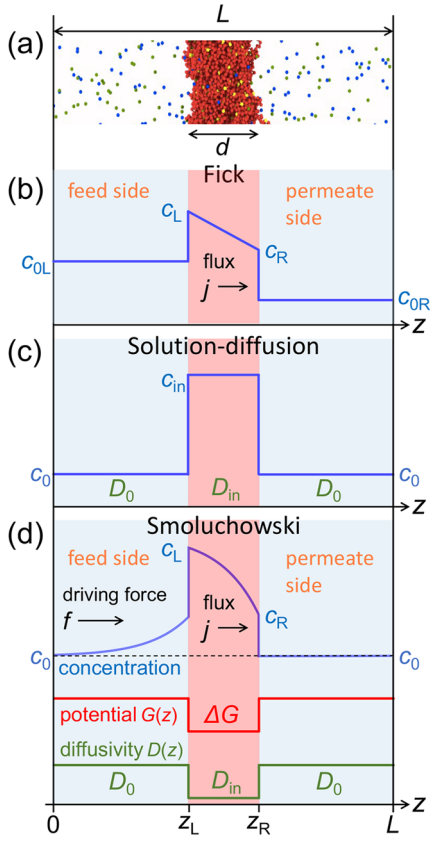


**Figure 1.** (a) Polymer network membrane (red) of thickness $d$, located at the center of a system of length $L$ with penetrants (small blue and green spheres). (b–d) Various scenarios of membrane permeation in a continuum representation. (b) Fick's type of permeation: The penetrant flux $j$ is generated by different bulk reservoir concentrations of penetrants $c_{0L}$ (feed side) and $c_{0R}$ (permeate side). (c) Solution–diffusion model with equilibrium penetrant concentrations $c_0$ in bulk and $c_{in}$ inside the membrane and corresponding diffusion coefficients $D_0$ and $D_{in}$. (d) Smoluchowski-type permeation in nonequilibrium: The penetrant flux $j$ is generated by a driving force $f$ (any forces apart from the Fick type) acting on penetrants, which flows from the feed side to the permeate side. $G(z)$ and $D(z)$ are the position-dependent membrane potential and diffusivity, respectively (see eqs 15 and 16).

of penetrant concentrations in the membrane ($c_{in}$) and the bulk reservoir ($c_0$), while $D_{in}$ is the diffusion coefficient of the penetrants in the membrane (see Figure 1(c)). Combining Fick's law with the partitioning $\mathcal{K}$, one finds $j = -D_{in}(c_R - c_L)/d = -D_{in}\mathcal{K}(c_{0R} - c_{0L})/d$, which relates boundary layer and bulk concentrations as sketched in Figure 1(b).

A relatively general starting point to describe transport for dense membranes is the Smoluchowski equation[60] (or the Fokker–Planck equation for overdamped dynamics[61−64]) of penetrants in the presence of a uniform force ($f$), also known as the "drift–diffusion equation".[65] This framework extends the classic solution–diffusion model to "inhomogeneous" solution–diffusion models,[52,66,67] where boundary layer effects and occurring nonlinearities can be captured. In this framework, the flux is generally described as

$$j = -D(z)\left[\frac{\mathrm{d}c(z)}{\mathrm{d}z} + \beta c(z)\left(\frac{\mathrm{d}G(z)}{\mathrm{d}z} - f\right)\right] \quad (3)$$

where the thermal energy is $k_BT = 1/\beta$. The first term of $j$ is the concentration gradient contribution (from Fick's law, as discussed above), the second term originates in the effective energy landscape of the membrane system, and the last term is due to the additional driving force. The latter generally represents any uniform driving force other than the former two contributions, such as external electrostatic, gravitational, and centrifugal forces,[68] or active forces as in biology.[69] The interpretation of $f$ as an electrostatic driving force leads to the Nernst–Plank equation for electromigration, the extension of which can model salt transport in reverse osmosis, including advection.[70] Our considerations also include the interpretation of $f$ as a low-Reynolds-number drag force from a uniform flow velocity, relevant for processes such as reverse osmosis.[8,66]

The potential field $G(z)$ constitutes the membrane as a finite energy barrier (or attractive well) in the system and originates from the microscopic interactions between penetrants and the membrane. We consider $G(z)$ as an average potential field, which can be obtained from molecular simulations by Boltzmann-inverting the average equilibrium partitioning profile.[71−76] The equilibrium diffusivity field $D(z)$ also depends on the membrane and penetrant properties. Our system comprises two local diffusivities, $D(z) = D_0$ in the bulk and $D(z) = D_{in}$ in the membrane (see eq 16). The latter depends on the penetrant–membrane interactions and membrane density.[72−74] The corresponding drift–diffusion scenario is depicted in Figure 1(d). Since we compare theoretical results with implicit-solvent computer simulations where no explicit solvent flow and drag are included (i.e., no hydrodynamics) and permeation is dominated by interaction potentials, the Smoluchowski equation given in eq 3 is the appropriate coarse-grained transport equation. This enables us to use equilibrium fields conveniently as input, which were calculated previously.[73] We resolve the reservoirs in both approaches, the Smoluchowski theory and simulations, to also obtain a microscopic view of concentration polarization effects in the important boundary layer[33,52,66,67] originating from the inhomogeneous density profiles of penetrants in the nonlinear large force regimes.

The aim of our work is to examine the behavior of transport and permeability in the nonlinear force regime in a driven system, by directly comparing solutions of the Smoluchowski equation to implicit-solvent molecular dynamics simulations of penetrants driven through a monomer-resolved polymer network membrane in contact with large reservoirs. We thus extend our previous theoretical work on equilibrium permeability[71−73,77] to nonequilibrium scenarios. We compare emerging penetrant profiles and fluxes and, in particular, seek reasonable definitions of $f$-dependent permeabilities in the system out of equilibrium, in which physical quantities under consideration reduce to equilibrium ones in the limit of $f \to 0$. We define "differential permeability" that substitutes for the linear equilibrium permeability in the flux–force relation (see the Theory section for more details). This enables us to further investigate to what extent the force can selectively control the permeability of one penetrant species with respect to the other in ideal binary mixtures. We demonstrate that our theoretical predictions agree well with the simulation results for this nonequilibrium model membrane transport. Importantly, we rationalize how differential permselectivity can be tuned by $f$, which provides experimentalists with additional means to better control solute transport as well as to describe the membrane permeability and transport properties. Extensions of


https://doi.org/10.1021/acs.macromol.2c00605
Macromolecules XXXX, XXX, XXX−XXX

our framework to ionic transport and (hydrodynamic) advection are possible, which are laid out in previous works as cited above.

## SIMULATION MODEL AND THEORY

**Simulation Model.** We perform Langevin dynamics simulations of cross-linked, semiflexible polymer networks in the presence of diffusive solutes (penetrants) driven by a force, as illustrated in Figure 2. The polymers form a random

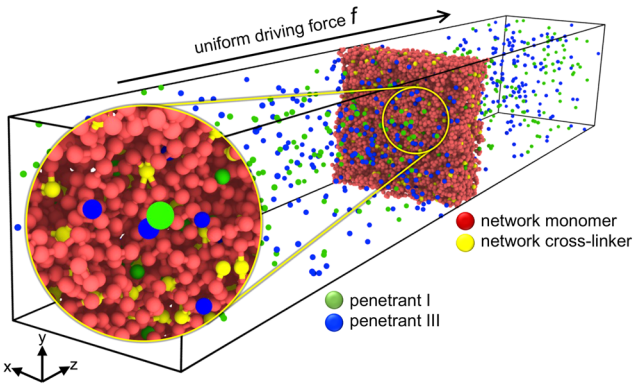


**Figure 2.** Simulation snapshot of a polymer network membrane in the presence of two types of diffusive penetrants (type $p_I$ in green, type $p_{III}$ in blue; type $p_{II}$ not included in this snapshot) driven by a uniform force $f$ in the $z$-direction (arrow). The polymers (red) are polydisperse in length and connected by tetrafunctional cross-linkers (yellow). The magnification circle shows the membrane structure in detail.

tetrafunctional network membrane in which the cross-linker fraction is around 5%.[73] The membrane is tethered at the center of the simulation box with harmonic constraints over the entire simulation time. The details of the membrane morphology, simulation setup, protocols, and coarse-grained (CG) force field parameters can be found in the Supporting Information as well as in our previous work on equilibrium permeability.[73]

Briefly, for nonbonded interactions, we consider Lennard-Jones (LJ) potentials $U_{LJ}^{ij}$ for $i, j$ = n or p, where n denotes the network particles (chain monomers and cross-linkers) and p stands for the penetrants. For the interactions between the penetrants, we use the LJ strength $\beta\epsilon_{pp} = 0.1$,[71−73] where the short-range and steep repulsion of the LJ potential dictates the interaction (steric exclusion limit). The intranetwork interaction $\epsilon_{nn}$ is interpreted as a measure of solvent quality[71−73,78] (thus controls the network volume fraction $\phi_n$). We use $\beta\epsilon_{nn} = 0.5$ in all our simulations, which yields $\phi_n \approx 0.17-0.23$ in equilibrium ($f = 0$), depending on $\beta\epsilon_{np}$. In this polymer density range, the permeability is strongly tunable by the network−penetrant interaction $\beta\epsilon_{np}$.[73] In this work, we consider three different penetrant types (termed $p_I$, $p_{II}$, and $p_{III}$) for which we use $\beta\epsilon_{np_I} = 0.1$, $\beta\epsilon_{np_{II}} = 0.6$, and $\beta\epsilon_{np_{III}} = 1.2$, as shown in Table 1. We consider one-component systems as well as mixtures (see Figure 2), namely, "mixture 1" of $\{p_I, p_{III}\}$ and "mixture 2" of $\{p_{II}, p_{III}\}$. The unit length $\sigma$ is used in the model, which is the particle diameter identical for all particles. The system's longitudinal length $L = 305\sigma$ is fixed for all systems under consideration. Table 1 summarizes the used $\beta\epsilon_{np}$ parameters in this study and the outcomes of equilibrium

**Table 1. Equilibrium Properties of the System for the Different Penetrant Types $p_I$, $p_{II}$, and $p_{III}$, Defined by the Network−Penetrant Interaction Strength $\beta\epsilon_{np}$: Equilibrium Membrane Permeability $\mathcal{P}^{eq}$, Penetrant Inner-Membrane Diffusivity $D_{in}$, Partitioning $\mathcal{K}$, and the Equilibrium Membrane Thickness $d/\sigma$, Where $D_0$ Is the Penetrant-Free Diffusivity in the Bulk Reservoir**

| penetrant type | $\beta\epsilon_{np}$ | $\mathcal{P}^{eq}/D_0$ | $D_{in}/D_0$ | $K$ | $d/\sigma$ |
|---|---|---|---|---|---|
| $p_I$ | 0.1 | 0.13 | 0.36 | 0.36 | 14.2 |
| $p_{II}$ | 0.6 | 0.40 | 0.26 | 1.54 | 14.6 |
| $p_{III}$ | 1.2 | 3.30 | 0.13 | 25.4 | 22.4 |

($f = 0$) penetrant partitioning, diffusivity, and membrane thickness values as determined previously.[73] In fact, the membrane thickness can vary with force. However, in our tethered membrane systems, the mean force-dependent membrane thickness, computed based on the full width at half-maximum, is nearly constant (see Figure S3 in the Supporting Information). We find one relatively large membrane thickness increase, for the highest force ($f = 1\ k_BT/\sigma$) and attractive penetrants ($p_{III}$), in which ∼10% chain stretching is found in comparison with the equilibrium value.

We apply a constant (in both space and time) force $f$ to all penetrants in the $z$-direction (see the arrow in Figure 2) for a sufficiently long time, ensuring a steady state where the penetrants' flux $j(z, f)$ is independent of $z$, i.e., constant (see the Supporting Information). For varying $f$, we analyze time-averaged penetrant concentration profiles $c(z, f)$, velocity profiles $v_z(z, f)$ in the $z$-direction, and thus the mean flux $j(f) = \langle c(z, f)v_z(z, f)\rangle$ as main quantities to describe the force-dependent permeability and selectivity. Here $\langle X\rangle = \int dz X/L$ denotes the average over the longitudinal space, where $L$ is the system length in the $z$-direction.

**Theory.** *One-Dimensional Steady-State Solutions of the Smoluchowski Equation.* To connect the simulations with the continuum transport theory, we utilize the system's homogeneity in the $xy$-directions, which allows us to project the observables onto one dimension (1D) along the $z$-direction as illustrated in Figure 1. Since we work at low densities of short-ranged repulsive penetrants, we can safely assume that the penetrants behave as an ideal gas in a 1D energy landscape; thus the governing equations are decoupled for different penetrant species. Hence, we consider ideal penetrants in a total potential $U(z, f) = G(z) - fz$ in 1D with a constant force $f$ and a position-dependent diffusivity $D(z)$. We recall the steady-state Smoluchowski equation introduced in eq 3 from which the steady-state flux $j$ with boundary conditions $c(z_1) = c_1$ and $c(z_2) = c_2$ yields the constant flux,[63,79]

$$j = \frac{c_1 e^{\beta U(z_1,f)} - c_2 e^{\beta U(z_2,f)}}{I(z_1, z_2, f)} \tag{4}$$

with

$$I(z_1, z_2, f) \equiv \int_{z_1}^{z_2} dy \frac{e^{\beta U(y,f)}}{D(y)} \tag{5}$$

The general solution for the $z$- and $f$-dependent penetrant concentration leads to


https://doi.org/10.1021/acs.macromol.2c00605
Macromolecules XXXX, XXX, XXX−XXX

$$c(z,f) = e^{-\beta U(z,f)}\left[c_1 e^{\beta U(z_1,f)} - (c_1 e^{\beta U(z_1,f)} - c_2 e^{\beta U(z_2,f)})\frac{I(z_1,z,f)}{I(z_1,z_2,f)}\right] \quad (6)$$

**Flux, Fick's Law, and Linear Response.** The flux obtained in eq 4 is a nonlinear function of $f$. We now briefly discuss the nature of $j$ and its connection to Fick's law, the solution−diffusion linear response, and permeability. To this end, consider a membrane-only system with a constant potential ($\Delta G$) and constant diffusivity ($D_{in}$) in the range of $z_L \le z \le z_R = z_L + d$ (i.e., a membrane of thickness $d$). This yields the total potential $U(z,f) = \Delta G - fz$, and one finds from eq 4 the exact expression

$$j = D_{in}\beta f \frac{c(z_L) - c(z_R)e^{-\beta f d}}{1 - e^{-\beta f d}} \quad (7)$$

where $c(z_L)$ and $c(z_R)$ are the penetrant concentrations at both boundaries. The nonlinearity of $j(f)$ is explicitly seen. Expressing in terms of a Taylor series for $f$, eq 7 reads

$$j = -\frac{D_{in}\Delta c}{d} + \frac{1}{2}D_{in}\{c(z_L) + c(z_R)\}\beta f - \frac{d}{12}D_{in}\Delta c(\beta f)^2 + \Delta c O(f^4) \quad (8)$$

with the concentration difference denoted by $\Delta c = c(z_R) - c(z_L)$. The first term (zeroth order of $f$) reveals Fick's law, which defines the solution−diffusion equilibrium membrane permeability (see eq 1) for $f = 0$, where the flux is driven by $\Delta c$ in nonequilibrium. The second term indicates the linear relation between $j$ and $f$, which is proportional to the arithmetic mean of the boundary concentrations, $[c(z_L) + c(z_R)]/2$. For vanishing $\Delta c$, the second term in eq 8 is the only nonvanishing term. This implies that when the penetrant's inner-membrane boundary concentrations are $c(z_L) = c(z_R) \equiv c_{in}$ in equilibrium, the nonlinear flux, $j$ in eq 7, explicitly reduces to the linear function

$$j = D_{in}c_{in}\beta f \quad (9)$$

In this limit, the flux inside the membrane is described by the equilibrium quantities $D_{in}$ and $c_{in}$ as a linear response to $f$, and a linear response permeability can be unambiguously defined.

**Definition of a System Permeability beyond Linear Response.** By using the equilibrium membrane permeability defined in eq 2, for which from now on we denominate $\mathcal{P}^{eq} = D_{in}c_{in}/c_0$ with the explicit superscript "eq", one finds from eq 9

$$j = \mathcal{P}^{eq}c_0\beta f \quad (10)$$

Equation 10 provides an important $j$−$f$ relation that defines $\mathcal{P}^{eq}$ as the proportionality factor on the linear response level, whereas the solution−diffusion model defines $\mathcal{P}^{eq}$ in the $j$−$\Delta c$ relation.

We now seek to extend the concept of permeability beyond linear response in our generic model framework. In this case, the system consists of a membrane immersed in the reference bulk reservoir of solutes (see Figures 1(d) and 2). A steady-state flux, $j(f)$, measured in this system is constant throughout space and time, regardless of being measured in the membrane or in the bulk reservoir. We thus bring forward the system's total permeability, $\mathcal{P}_{sys}$, defined in a general fashion as the proportionality factor of the system's observable $j(f)$ via

$$j(f) \equiv \mathcal{P}_{sys}(f)c_0\beta f \quad (11)$$

This inspires us to define a force-dependent *chordal* or *mean* system permeability,

$$\mathcal{P}_{sys}(f) \equiv \frac{j(f)}{c_0\beta f} \quad (12)$$

which shares the same philosophy as an $f$-dependent mobility $\mu(f) = v(f)/f$ defined as the apparent prefactor of the velocity $v$ with respect to the force.[63,80] In addition, we consider another quantity for permeation, defining the *incremental* or *differential* system permeability as

$$\mathcal{P}^{\Delta}_{sys}(f) \equiv \frac{1}{c_0\beta}\frac{dj(f)}{df} \quad (13)$$

which is analogous to the definition of differential conductivity in charge transport in other systems, such as semiconductors or lattice gases.[81−83] It describes the change of the flux with respect to isothermal incremental changes of $f$. Both quantities, $\mathcal{P}_{sys}$ and $\mathcal{P}^{\Delta}_{sys}$, coincide in the force-free limit ($f \to 0$); that is, they are independent of $f$ (linear response). However, as we will quantify, they can be $f$-dependent and different in higher force regimes in general.

In this work, we differentiate between $\mathcal{P}_{sys}(f)$ and $\mathcal{P}^{\Delta}_{sys}(f)$ by terming the former simply "system permeability" and the latter explicitly "differential system permeability". The latter is particularly a new concept to define permeability. Note that the defined quantities correspond to a total system permeability, not the individual membrane permeability in contact with a solute reservoir. Only in equilibrium, because of the linearity of the system, the bulk permeability and the membrane permeability, $\mathcal{P}^{eq}$, can be defined individually and simply added reciprocally to obtain the equilibrium system permeability, $\mathcal{P}^{eq}_{sys}$ (like resistances in an electric circuit; see ref 52 or our discussion later around eq 27). Beyond linear response, the global flux is determined by the membrane properties, system size, and boundary conditions in a nonadditive fashion.

**Penetrant Concentration Profiles for the Membrane-Only Case.** The penetrant concentration for the above membrane-only case leads from eq 6 to

$$c(z,f) = c(z_L) + \Delta c\frac{1 - e^{\beta f(z-z_L)}}{1 - e^{\beta f d}} \quad (14)$$

which reduces to the limiting expressions $c(z) = c(z_L) + \Delta c(z - z_L)/d$ for $f \to 0$ and $c(z) = c(z_L)$ in the range of $z_L \le z < z_R$ for $f \to \infty$ (see Figure S4 in the Supporting Information for more details of $c(z,f)$ for the membrane-only case).

## RESULTS AND DISCUSSION

**Single-Component Penetrant System.** Equipped with the general steady-state solutions and definitions, let us now consider a special system of a membrane with a bulk reservoir of penetrants (see Figure 1(d)), for which we assume a piecewise constant form for both the potential and the diffusivity, according to


https://doi.org/10.1021/acs.macromol.2c00605
Macromolecules XXXX, XXX, XXX−XXX

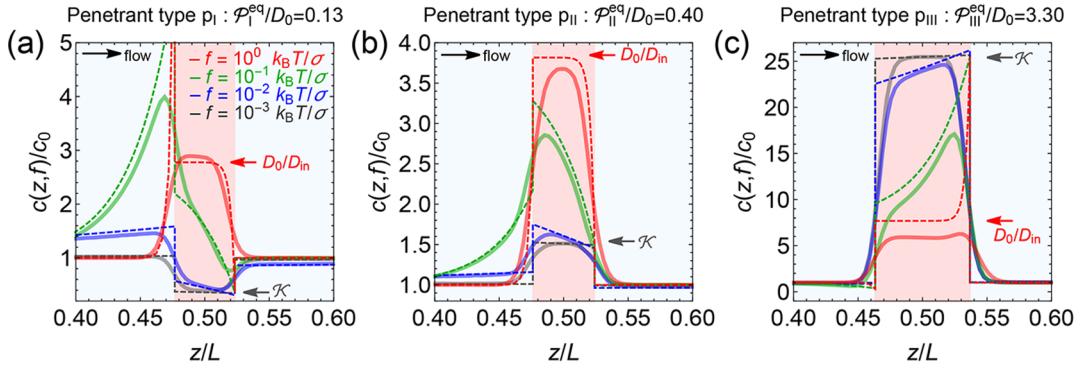


**Figure 3.** Normalized penetrant concentration profiles $c(z,f)/c_0$ in single-component penetrant systems for different forces. The red-shaded area depicts the membrane region with equilibrium thickness $d$. The time-averaged steady-state profiles from the simulation results (solid lines) and the theoretical prediction (dashed lines) from the steady-state Smoluchowski solution (eq 18) are compared for different parameters (a) $\beta\epsilon_{np_I} = 0.1$ and $\mathcal{P}_I^{eq}/D_0 = 0.13$, (b) $\beta\epsilon_{np_{II}} = 0.6$ and $\mathcal{P}_{II}^{eq}/D_0 = 0.4$, and (c) $\beta\epsilon_{np_{III}} = 1.2$ and $\mathcal{P}_{III}^{eq}/D_0 = 3.3$. The arrows depict the limiting values for the penetrant's inner-membrane concentration, $c_{in}/c_0 = \mathcal{K}$ for $f \to 0$ (gray, see eq 19), and $c_{in}(L/2)/c_0 = D_0/D_{in}$ for $f \to \infty$ (red, see eq 21). The used parameter values are summarized in Table 1. The standard error of the time-averaged concentration profiles obtained from the simulations is smaller than the line thickness.

$$G(z) = \begin{cases} \Delta G & z_L \le z \le z_R \\ 0 & \text{elsewhere} \end{cases} \tag{15}$$

and

$$D(z) = \begin{cases} D_{in} & z_L \le z \le z_R \\ D_0 & \text{elsewhere} \end{cases} \tag{16}$$

with $z_L = L/2 - d/2$ and $z_R = L/2 + d/2$. The penetrants are of one kind (single-component), driven by a force $f$, and have the same bulk concentrations at both system boundaries $c(0) = c(L) = c_0$. The solution $c(z)$ conforms to the imposed boundary condition for $G(z)$ and $D(z)$, which is periodic in the $z$-direction with the period $L$.[63] This enables the comparison with the simulation results in which periodic boundary conditions are used.

In our previous work, we have obtained $G(z)$ from simulations in equilibrium via $\beta G(z) = -\ln[c^{eq}(z)/c_0^{eq}]$ where $c^{eq}(z)$ and $c_0^{eq}$ are the penetrant's equilibrium concentration profile and the bulk concentration, respectively.[72−74] We observed that $G(z)$ can be conveniently mapped on a piecewise step function given in eq 15. The mean plateau value of $G(z)$ in the membrane, $\Delta G$, defines our partition ratio (see Table 1) via

$$\Delta G = -k_BT \ln \mathcal{K} \tag{17}$$

A similar piecewise mapping is assumed for the diffusivity field as in eq 16, of which $D_{in}$ and $D_0$ were previously studied in equilibrium.[72−76]

**Penetrant Concentration Profiles.** It is straightforward to obtain the penetrant concentration profile from the general solution eq 6, reading

$$\frac{c(z,f)}{c_0} = \left[1 - (1 - e^{-\beta f L})\frac{I(0,z,f)}{I(0,L,f)}\right] e^{-\beta U(z,f)} \tag{18}$$

The full closed-form expression of eq 18 is presented in the Supporting Information, where the penetrant concentrations are denoted by the following subscripts depending on the location,

$$c(z,f) = \begin{cases} c_{0L}(z,f) & 0 \le z < z_L \\ c_{in}(z,f) & z_L \le z \le z_R \\ c_{0R}(z,f) & z_R < z \le L \end{cases}$$

In Figure 3, we compare $c(z,f)/c_0$ from the simulations (solid lines) with the theoretical prediction (eq 18, dashed lines) for the single-component-penetrant−membrane systems. We visualize the membrane region as red-shaded areas with equilibrium thickness $d$ (see Table 1 and Methods in the Supporting Information). We notice at first glance that our continuum-level theory based on the piecewise potential model is overall in remarkable agreement with our particle-based CG simulation results for the highly inhomogeneous density profiles, for different forces and network−penetrant interaction parameters $\epsilon_{np}$.

For the repulsive network−penetrant interactions with the penetrants of type $p_I$ ($\beta\epsilon_{np_I} = 0.1$), yielding the smallest equilibrium membrane permeability ($\mathcal{P}_I^{eq}/D_0 = 0.13$) in the chosen parameter set, the change of $c(z,f)$ upon increasing $f$ is significant, as shown in Figure 3(a). Since the network−penetrant interaction is repulsive, the global magnitude of the penetrant's inner-membrane concentration ($c_{in}(z,f)$) is smaller than in the reservoir bulk regions ($c_{0L}(z,f)$ and $c_{0R}(z,f)$); thus $\mathcal{K} < 1$, for small forces up to $\beta f = 0.01/\sigma$ close to equilibrium. As the force further increases, a dramatic inversion of $c(z,f)$ occurs, in which the penetrants infiltrate into the membrane much more, eventually resulting in the increase of the system's permeability (as discussed further below). In particular, under the intermediate force, $\beta f = 0.1/\sigma$, a giant penetrant accumulation around the left (feed) side of the membrane−reservoir interface is observed, which even exceeds the inner concentration $c_{in}(z,f)$, as depicted by the green line in Figure 3(a). This induces a rapidly decaying concentration profile $c_{in}(z,f)$ that becomes extremely inhomogeneous in this intermediate force regime, which decays even below the bulk concentration at the right (permeate) side of the membrane. Hence, we provide a microscopic view of concentration polarization effects in the boundary layer.[33]


https://doi.org/10.1021/acs.macromol.2c00605
Macromolecules XXXX, XXX, XXX−XXX

For the slightly attractive network−penetrant interactions with the penetrants of type $p_{II}$ ($\beta\epsilon_{np_{II}} = 0.6$), yielding $\mathcal{P}^{eq}_{II}/D_0 = 0.4$ but still less than unity (see Figure 3(b)), the penetrant's interfacial accumulation around the feed side is observed again under the intermediate $f$ (the green line). However, there is no dramatic inversion of $c_{in}(z,f)$ with respect to the bulk concentrations as $f$ varies. This tendency is related to the partitioning, which is $\mathcal{K} > 1$ in this case. The penetrant's inner-membrane concentration tends to increase as $f$ increases and decay under the intermediate force, similar to the results in Figure 3(a).

The above observed feed-side interfacial accumulation implies a penetrant's congestion due to the intrinsically low permeability of the membrane, i.e., low $D_{in}$ and low $\mathcal{K}$. This jamming at the entry is released by a sufficiently large force that compensates for the penalty from the low permeability and eventually becomes negligible under higher forces. For example, in the case of Figure 3(a), the maximal feed-side accumulation occurs at $\beta f = 0.1/\sigma$. The potential barrier height in this case is $\beta\Delta G = -\ln \mathcal{K} \approx 1$. This is comparable to the energy needed to move a penetrant over a distance of the membrane thickness ($d/\sigma \approx 14$) with $\beta f = 0.1/\sigma$, which amounts to $\beta f d \approx 1.4$. Thus, there occurs a large interfacial accumulation. The interfacial accumulation is released with the larger force $\beta f = 1/\sigma$, which corresponds to the membrane-crossing energy $\beta f d \approx 14$, which is over 10-fold larger than $\beta\Delta G$.

For the more attractive network−penetrant interactions with the penetrants of type $p_{III}$ ($\beta\epsilon_{np_{III}} = 1.2$) yielding $\mathcal{P}^{eq}_{III}/D_0 = 3.3$ and now larger than unity (see Figure 3(c)), we find a significantly different behavior of $c(z,f)$. First, owing to the negative energy barrier arising from the membrane, there is no salient interfacial accumulation of the penetrants. Second, the magnitude of $c_{in}(z,f)$ decreases with $f$, which reduces partitioning but the flux increases. Lastly, now $c_{in}(z,f)$ increases with $z$, thereby having a positive gradient $dc_{in}(z,f)/dz > 0$. This positive gradient signifies a flux in the $z$-direction against the concentration gradient, which is often found in biophysics, featuring active transport.[84,85] Note that, however, this feature is found only for the intermediate $f$, whereas the high force regime renders rather a flat concentration profile, $c_{in}(z,f)$, whose shape seldomly affects the flux. The sign change of the concentration gradient depends on $\mathcal{P}^{eq}$. We find the threshold of this sign change at $\mathcal{P}^{eq} = D_0$, which is evident from $dc_{in}(z,f)/dz \propto (\mathcal{P}^{eq} - D_0)$.

The limiting expressions for the concentration $c(z,f)$ reduce to

$$c(z) = \begin{cases} c_0\mathcal{K} & z_L \le z \le z_R \\ c_0 & \text{elsewhere} \end{cases} \tag{19}$$

not only for $f \to 0$ (see the gray arrows in Figure 3) but also when the membrane is as permeable as the bulk (that is, $\mathcal{P}^{eq} = D_0$). In addition, we find a leading-order expression for the penetrant concentration at the center of the membrane

$$\frac{c_{in}(L/2)}{c_0} = \mathcal{K}e^{-\beta f d/2} + \frac{D_0}{D_{in}}(1 - e^{-\beta f d/2}) \tag{20}$$

which reduces to a notable limiting expression

$$\lim_{f\to\infty} \frac{c_{in}(L/2)}{c_0} = \frac{D_0}{D_{in}} \tag{21}$$

Therefore, the penetrant's membrane diffusivity in equilibrium can be estimated by measuring the nonequilibrium concentration ratio under a high $f \gg k_BT/d$ (see the red arrows in Figure 3). This analytical result is important because it provides information on the equilibrium inner-membrane diffusivity $D_{in}$ by applying a high force $f$, particularly useful to measure intrinsically extremely low $D_{in}$. We observe the onset of the qualitative agreement between eq 21 and simulation results at $f = 1\ k_BT/\sigma$. This reference high force, e.g., for a colloid particle of size 1 $\mu$m at 300 K, yields $f = 1\ k_BT/\mu m \approx 0.026$ eV/$\mu$m, which amounts to an electric field of 260 V/cm per electric charge 1$e$. This is in the range of feasible electric field strengths in electrophoresis experiments.[86]

Overall, the simple continuum-level Smoluchowski picture agrees very well qualitatively and even semiquantitatively with the simulation results for $c(z,f)$. However, the theory exhibits limitations. The quantitative deviations from the simulation results can be attributed to the complexity arising from the polymer network membrane. The membrane is not a simple homogeneous medium. In stark contrast, it exhibits force- and location-dependent (volume) responses, especially with high forces and strong attractions. The latter features would also be dominant with many-body effects in highly collapsed membranes, which makes our theoretical prediction challenging. Moreover, the simulated membrane−bulk system does not provide a piecewise constant landscape ($G(z)$, $D(z)$) as ideally imposed in the theory, leading to the largest differences between the two approaches at the interfaces. Nevertheless, our simple theory is qualitatively valid for the force range we consider in this study.

***f*-Dependent Flux and System Permeabilities.** Now we focus on the steady-state flux $j$, obtained in a closed form as a nonlinear function of $f$ (see the Supporting Information for derivation),

$$j = D_0c_0\beta f\left[1 + \left(\frac{D_0}{\mathcal{P}^{eq}} - 1\right)S(f)\right]^{-1} \tag{22}$$

where $S(f) \equiv \sinh(\beta f d/2)/\sinh(\beta f L/2)$. This nonlinear $j$−$f$ relation is remarkably simple and important because once $j(f)$ is measured from experiments, it is straightforward to calculate the intrinsic membrane permeability $\mathcal{P}^{eq}$ determined solely by the known equilibrium parameters $\beta$, $c_0$, and $D_0$ and the system dimension parameters $d$ and $L$. Note that at $\mathcal{P}^{eq}/D_0 = 1$, the nonlinear term in eq 22 vanishes and the flux becomes a linear function of $f$.

The flux has no zeroth-order term of $f$ (cf. eq 8), and the leading-order term for small force $f \ll k_BT/L \ll k_BT/d \ll k_BT/\sigma$ yields

$$j^{lin} = D_0c_0\beta f\left[1 + \left(\frac{D_0}{\mathcal{P}^{eq}} - 1\right)\frac{d}{L}\right]^{-1} \tag{23}$$

Another important feature of $j$ is found in the high force regime, where the membrane as an energy barrier becomes unimportant. The flux simply reduces to the relation for the homogeneous bulk solution

$$j^{\infty} = D_0c_0\beta f \tag{24}$$


https://doi.org/10.1021/acs.macromol.2c00605
Macromolecules XXXX, XXX, XXX−XXX

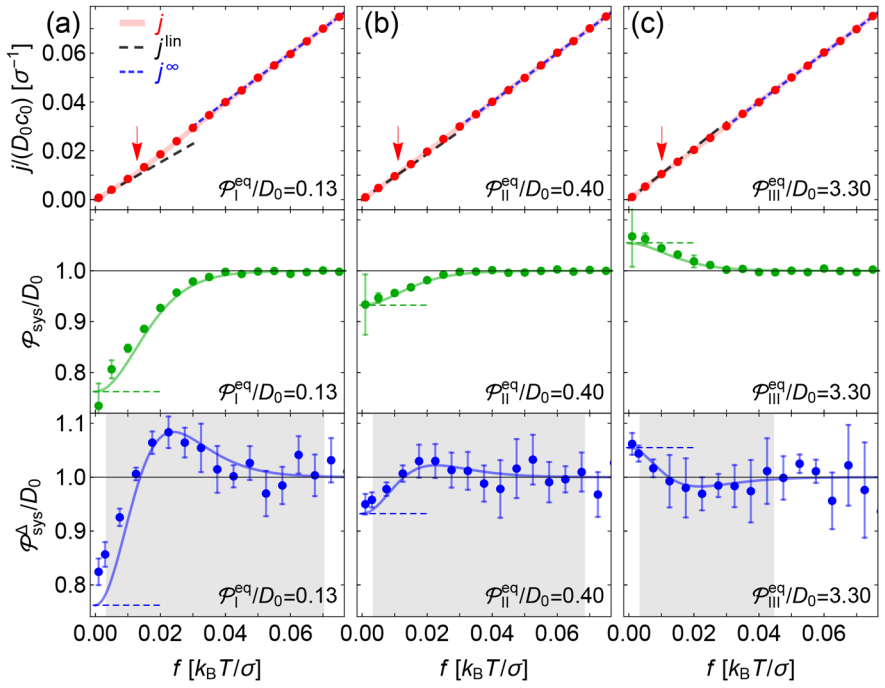


**Figure 4.** Nonequilibrium flux and permeability results for the single-component penetrant systems, presented for the three penetrant types (cf. Table 1) of different equilibrium membrane permeabilities (a) $\mathcal{P}_{\mathrm{I}}^{\mathrm{eq}}/D_0 = 0.13$, (b) $\mathcal{P}_{\mathrm{II}}^{\mathrm{eq}}/D_0 = 0.4$, and (c) $\mathcal{P}_{\mathrm{III}}^{\mathrm{eq}}/D_0 = 3.3$. Top panels: steady-state flux $j(f)/(D_0c_0)$ from the exact solution (red solid lines, see eq 22), the leading-order expression $j^{\mathrm{lin}}$ (black dashed lines, see eq 23), and $j^{\infty}$ (blue dashed lines, see eq 24), compared with the simulation results (symbols). Middle panels: system permeability, $\mathcal{P}_{\mathrm{sys}} = j(f)/(c_0\beta f)$, normalized by $D_0$, obtained from the theory (solid lines, see eq 25) and simulations (symbols). Bottom panels: differential system permeability, $\mathcal{P}_{\mathrm{sys}}^{\Delta} = \mathrm{d}j(f)/(c_0\beta \mathrm{d}f)$ normalized by $D_0$, obtained from the theory and simulations. The horizontal dashed lines depict the limiting values of $\mathcal{P}_{\mathrm{sys}}^{\mathrm{eq}}$ for $f \to 0$ (see eq 26). The horizontal solid lines depict $\mathcal{P}_{\mathrm{sys}}/D_0 = \mathcal{P}_{\mathrm{sys}}^{\Delta}/D_0 = 1$. The arrows in the top panels depict the critical force, $f^*$, derived in eq 28, which signifies the force that triggers the nonlinear $j$. The gray-shaded regions in the bottom panels depict the range of $k_{\mathrm{B}}T/L \lesssim f \lesssim k_{\mathrm{B}}T/d$.

implying that the nonlinear nature of the flux $j$ lies in an intermediate range of the force, $k_{\mathrm{B}}T/L \lesssim f \lesssim k_{\mathrm{B}}T/d$ ($0.003 \lesssim f \lesssim 0.06\ k_{\mathrm{B}}T/\sigma$). Otherwise, the flux in both small and large $f$ limits is simply a linear function of $f$, i.e., $j^{\mathrm{lin}}$ or $j^{\infty}$.

In the top panels of Figure 4, the exact expression for the flux $j$ (red solid lines, eq 22), rescaled by $D_0c_0$, is compared with the leading-order expressions $j^{\mathrm{lin}}$ (eq 23) and $j^{\infty}$ (eq 24) as well as simulation results for $j = \langle c(z)v_z(z)\rangle$ (symbols), for different $\mathcal{P}^{\mathrm{eq}}$. The theoretical prediction for $j$ is in excellent agreement with the simulation results. The nonlinearity of $j$ is more significant for smaller $\mathcal{P}^{\mathrm{eq}}$ (Figure 4(a)). For $\mathcal{P}^{\mathrm{eq}} \gg D_0$ the flux is almost linear, as shown in the top panels of Figure 4(b) and (c).

In fact, the steady-state flux obtained in eq 22 is the system's flux embracing the bulk reservoir and the membrane. Using our definition, eq 12, we obtain the nonlinear, nonequilibrium system permeability,

$$\mathcal{P}_{\mathrm{sys}}(f) = D_0\left[1 + \left(\frac{D_0}{\mathcal{P}^{\mathrm{eq}}} - 1\right)S(f)\right]^{-1} \tag{25}$$

In the limit of $f \to 0$, we find that $\mathcal{P}_{\mathrm{sys}}$ reduces to the proportionality constant of the foregoing linear response $j^{\mathrm{lin}} = \mathcal{P}_{\mathrm{sys}}^{\mathrm{eq}}c_0\beta f$ as

$$\mathcal{P}_{\mathrm{sys}}^{\mathrm{eq}} = D_0\left[1 + \left(\frac{D_0}{\mathcal{P}^{\mathrm{eq}}} - 1\right)\frac{d}{L}\right]^{-1} \tag{26}$$

which provides a relation between the system permeability and the membrane permeability in equilibrium. Rewritten, it reveals a known reciprocal summation rule for the equilibrium system permeability,[52]

$$\frac{L}{\mathcal{P}_{\mathrm{sys}}^{\mathrm{eq}}} = \frac{(L-d)/2}{\mathcal{P}_{0\mathrm{L}}^{\mathrm{eq}}} + \frac{d}{\mathcal{P}^{\mathrm{eq}}} + \frac{(L-d)/2}{\mathcal{P}_{0\mathrm{R}}^{\mathrm{eq}}} \tag{27}$$

with the equilibrium bulk permeability denoted by $\mathcal{P}_{0\mathrm{L}}^{\mathrm{eq}} = \mathcal{P}_{0\mathrm{R}}^{\mathrm{eq}} = D_0$. In addition, in the limit of $f \to \infty$, we find $\mathcal{P}_{\mathrm{sys}}^{\infty} = D_0$, where the effect of the membrane vanishes.

In the middle horizontal panels of Figure 4, the theoretical prediction for $\mathcal{P}_{\mathrm{sys}}(f)$ obtained in eq 25 is depicted by the solid line, showing very good agreement with the simulation results analyzed from $\langle c(z, f)v_z(z, f)\rangle/(c_0\beta f)$ (symbols). The system permeability, $\mathcal{P}_{\mathrm{sys}}(f) = j/(c_0\beta f)$, monotonically increases or decreases with $f$ from the equilibrium value ($\mathcal{P}_{\mathrm{sys}}^{\mathrm{eq}}$) to the limiting value $\mathcal{P}_{\mathrm{sys}}^{\infty} = D_0$. This change of $\mathcal{P}_{\mathrm{sys}}(f)$, signifying the nonlinearity of $j$, indeed mostly occurs in the range of $k_{\mathrm{B}}T/L \lesssim f \lesssim k_{\mathrm{B}}T/d$. We note that we found a closed-form solution for the nonequilibrium differential system permeability via our definition $\mathcal{P}_{\mathrm{sys}}^{\Delta}(f) = \mathrm{d}j/(c_0\beta \mathrm{d}f)$ (see eq S11 in the Supporting Information for the full closed-form expression).

In the bottom panels of Figure 4, the analytical results for $\mathcal{P}_{\mathrm{sys}}^{\Delta}(f)$ are compared with the discrete derivatives of the simulation data for $j$. The major characteristics of $\mathcal{P}_{\mathrm{sys}}^{\Delta}$, i.e., a


https://doi.org/10.1021/acs.macromol.2c00605
Macromolecules XXXX, XXX, XXX−XXX

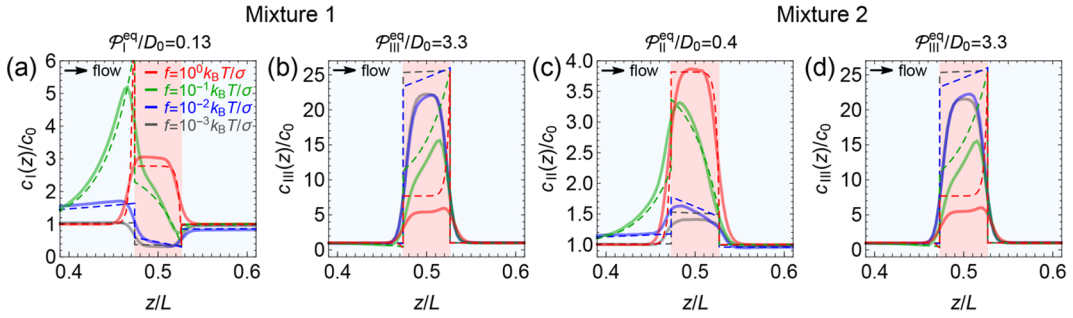


**Figure 5.** Penetrant concentration profiles in the two-component penetrant mixtures (mixture 1 of $\{p_I, p_{III}\}$ and mixture 2 of $\{p_{II}, p_{III}\}$), presented for different forces. The red-shaded areas depict the membrane regions with equilibrium thicknesses $d/\sigma = 16$ and $d/\sigma = 16.4$ for mixtures 1 and 2, respectively. The simulation results (solid lines) and the theoretical predictions (dashed lines) from the steady-state Smoluchowski solution (eq 18) are compared for different parameters for mixture 1 with (a) $\{\beta\epsilon_{npI} = 0.1,\ \mathcal{P}_I^{eq}/D_0 = 0.13\}$ and (b) $\{\beta\epsilon_{npIII} = 1.2,\ \mathcal{P}_{III}^{eq}/D_0 = 3.3\}$ and for mixture 2 with (c) $\{\beta\epsilon_{npII} = 0.6,\ \mathcal{P}_{II}^{eq}/D_0 = 0.4\}$ and (d) $\{\beta\epsilon_{npIII} = 1.2,\ \mathcal{P}_{III}^{eq}/D_0 = 3.3\}$.

*differential* response function of $f$, reveal that the nonlinear response of the flux is a dramatically varying, nonmonotonic function of $f$, particularly for less permeable systems. This reflects that the penetrants' response in terms of the permeability can be largely controlled by $f$. The critical force ($f^*$), which maximizes the nonlinearity, is obtained by solving $d\mathcal{P}_{sys}^{\Delta}(f)/df = 0$ as

$$f^* = 6\sqrt{\frac{2}{7}}k_BT\left[\frac{1}{L} + \frac{5}{7}\left(\frac{D_0}{\mathcal{P}^{eq}} - 1\right)\frac{d}{L^2}\right] \tag{28}$$

approximated for $d \ll L$ and $f \ll k_BT/d$. This leading-order expression of $f^*$, which triggers the nonlinear flux (thus permeability), reveals its lower bound determined by $\sim k_BT/L$. The corresponding $f^*$ are depicted by vertical arrows in Figure 4.

We note here that our finding of the nonmonotonic nature of $\mathcal{P}_{sys}^{\Delta}(f)$ bears a resemblance to the effective diffusivity found in ideal 1D tilted periodic potentials.[87−91] It turned out that a small free diffusion coefficient of a particle (e.g., a particle with high friction) can accelerate its mobility in washboard-like potentials when optimally tilted. This tendency is similar to our finding that the maximum of the differential system permeability is enhanced with a low equilibrium membrane permeability, with $D_0$ being fixed. In fact, we observe in the range of $k_BT/L \lesssim f \lesssim k_BT/d$ a large nonmonotonicity of $\mathcal{P}_{sys}^{\Delta}(f)$, apparently corresponding to the resonant critical force[88] in the washboard systems. This feature may be more generally observable and important in other systems (such as in biophysics and electrical engineering), providing a clue to tunable permeability and selectivity by the force $f$ in membrane applications.

Further inspection of the nonmonotonicity of $\mathcal{P}_{sys}^{\Delta}(f)$ is worthwhile in connection with the penetrant concentration profile: from the results in Figure 4(a) and (b), it turns out that the intermediate force $\beta f = 0.1/\sigma$, which induces the notable feed-side accumulation of the penetrants (cf., Figure 3(a) and (b)), is actually high enough for approaching fully linear flux ($j^{\infty}$) and thus $\mathcal{P}_{sys}^{\Delta} = D_0$. The maximal response of $\mathcal{P}_{sys}^{\Delta}(f)$ arises at around $\beta f = 0.02/\sigma$ (see the peaks at the bottom panels of Figure 4(a) and (b)). Here, the penetrants accumulate on the feed-side interface, which builds asymmetry between $c_{0L}(z, f)$ and $c_{0R}(z, f)$ across the membrane toward the permeate side, resulting in the gradually decreasing concentration gradient (see the blue lines in Figure 3(a) and (b)). This balance between the bulk concentration asymmetry and the moderate linear gradient of the inner-membrane concentration (close to Fick's type permeation shown in Figure 1(b)) is sensitively modulated by changing the force by a small amount, which largely tunes the permeability. In this force regime, thus the differential system permeability is maximized, assisted by the force ($f$) and the concentration difference ($\Delta c$) in a cooperating fashion (see eq 8 and subsequent discussions). It is interesting to observe the opposite feature in Figure 4(c): $\mathcal{P}_{sys}^{\Delta}(f)$ is minimized at around almost the same small optimal force ($\beta f = 0.02/\sigma$) at which the gradual increase of $c_{in}$ occurs (see the blue line in Figure 3(c)). Thus, with the higher $\mathcal{P}^{eq}$ and the intermediate force, the differential system permeability is maximally hindered by the backward flux originated from the Fick-type mechanism dominated by the concentration gradient.

**Mixture of Two-Component Penetrants.** The objective of this section is to explore the feature of $f$-dependent selective permeation in a mixture of different penetrants, particularly examining the role of $f$ in the control of the permselectivity of the membrane. For our hard-sphere penetrants, we expect that the single-component Smoluchowski solutions are decoupled and additive; therefore our theory may apply for to mixtures. However, we cannot rule out membrane-mediated interactions between the penetrants, which can be tested by a comparison with the ideal Smoluchowski framework. For this, we consider two-component mixtures of penetrant types $p_I$, $p_{II}$, and $p_{III}$. In mixture 1 composed of $\{p_I, p_{III}\}$, $p_I$ is repulsive to the membrane, and $p_{III}$ is strongly attractive, cf. Table 1. In mixture 2 of $\{p_{II}, p_{III}\}$, $p_{II}$ is moderately attractive to the membrane and $p_{III}$ is strongly attractive. For all cases, the penetrant−penetrant interaction is always repulsive (steric), as in the single-component systems.

*Penetrant Concentration Profiles.* In Figure 5, the simulation results for the penetrant concentration profiles $c_I(z)$ and $c_{III}(z)$ in each mixture are compared with the theoretical prediction (eq 18). The results exemplify that the decomposed Smoluchowski picture applies even for the mixtures in which we consider only mutually repulsive penetrants and the equilibrium membrane permeability up to $\mathcal{P}_{III}^{eq} \approx 3D_0$. But we also observe a limitation of the theory, especially for the highly attractive penetrant ($p_{III}$), which deviates more from the simulation results in comparison with


https://doi.org/10.1021/acs.macromol.2c00605
Macromolecules XXXX, XXX, XXX−XXX

the single-component cases. However, the main characteristics of the gradient change of $c_{in}(z, f)$ depending on $\mathcal{P}^{eq}$ with the corresponding threshold argument, $\mathcal{P}^{eq} = D_0$, are still validly captured by our theory. The discrepancies found in Figure 5(b) and (d) are expected because the polymer membrane system involves additional complex features in membrane responses and many-body correlations, which are not accounted for in the theory. Nevertheless, the result shows that our simple theory can also be utilized to characterize such cosolute mixtures, especially with low intrinsic (equilibrium) membrane permeabilities.

*f-Dependent Flux and System Permeabilities.* We show the analytical results for the flux, the system permeability, and the differential system permeability in Figure 6, compared with the simulation results. The fluxes in the mixtures exhibit overall a similar tendency to that observed in the single-component system, in which the nonlinearity with respect to $f$ is more significant for intrinsically less permeable penetrants, $p_I$. The comparison of $j$ demonstrates the validity of the prediction, eq 22, for the two-component mixture, which even quantitatively

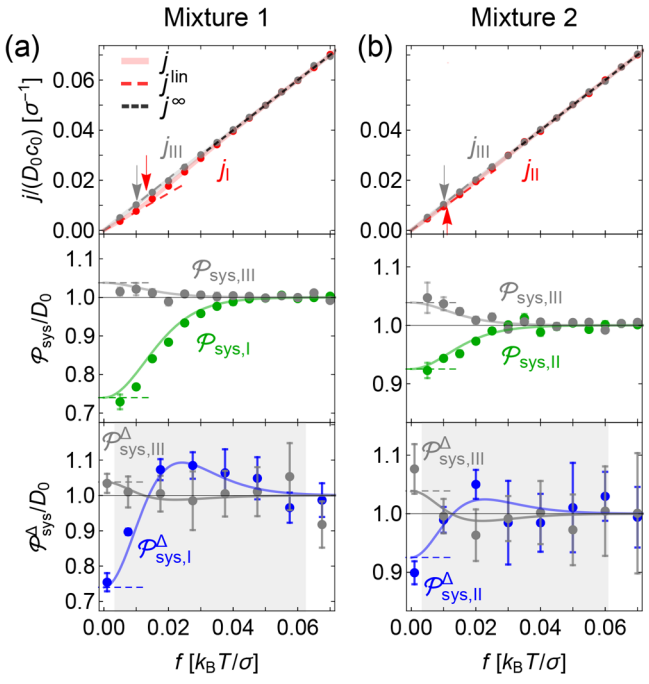


**Figure 6.** Results for flux and permeabilities for the two-component penetrant mixtures, for (a) mixture 1: $\mathcal{P}^{eq}_I/D_0 = 0.13$, $\mathcal{P}^{eq}_{III}/D_0 = 3.3$ and (b) mixture 2: $\mathcal{P}^{eq}_{II}/D_0 = 0.4$, $\mathcal{P}^{eq}_{III}/D_0 = 3.3$. Top panels: steady-state flux $j(f)/(D_0c_0)$ from the exact solution (red and gray solid lines, see eq 22), $j^{lin}$ (red and gray dashed lines), and $j^{\infty}$ (black dashed lines), compared with the simulation results (symbols). Middle panels: system permeability $\mathcal{P}_{sys} = j(f)/(c_0\beta f)$ normalized by $D_0$, obtained from the theory (solid lines, see eq 25) and simulations (symbols). Bottom panels: differential system permeability, $\mathcal{P}^{\Delta}_{sys} = dj(f)/(c_0\beta df)$ normalized by $D_0$, obtained from the theory (solid lines) and simulations (symbols). The horizontal dashed lines depict the limiting values of $\mathcal{P}^{eq}_{sys}$ for $f \to 0$ (see eq 26). The horizontal solid lines depict $\mathcal{P}_{sys}/D_0 = \mathcal{P}^{\Delta}_{sys}/D_0 = 1$. The used parameter values are summarized in Table 1. The arrows in the top panels depict the critical force, $f^*$, derived in eq 28, which signifies the force that triggers the nonlinear $j$. The gray-shaded regions in the bottom panels depict the range of $k_BT/L \lesssim f \lesssim k_BT/d$.

matches with the simulation results, demonstrating the additivity within the chosen parameter sets. The system permeabilities (middle horizontal panels in Figure 6) first start at the equilibrium values ($\mathcal{P}^{eq}_{sys,I}$ and $\mathcal{P}^{eq}_{sys,III}$) for very small forces and gradually and monotonically converge to the bulk permeability $D_0$ for very large forces, which is similar to that separately found for the single-component system in Figure 4. Therefore, we confirm that this tendency for each permeability in the same mixture is effectively captured by our theory in a decomposed fashion.

The predicted differential system permeabilities $\mathcal{P}^{\Delta}_{sys}(f)$ (solid lines in bottom panels) also match well with the simulation results. The observed simultaneous occurrence of maximization and minimization of $\mathcal{P}^{\Delta}_{sys}(f)$ for the different penetrant types in the mixture reflects the immanence of selectivity that can be largely controlled by small changes of the force, particularly in the mixture with low permeability. In the shown range of the force, $0 < f \lesssim 0.06\ k_BT/\sigma$, $\mathcal{P}_{sys}$ and $\mathcal{P}^{\Delta}_{sys}$ converge to $D_0$ for large forces, which is associated with the membrane width via $k_BT/L \lesssim f \lesssim k_BT/d$: The used parameter value $d \approx 16\sigma$ corresponds to $f \approx 0.06\ k_BT/\sigma$.

**System Selectivity.** We now consider the system selectivity as the ratio between two system permeabilities, $\alpha_{sys} \equiv \mathcal{P}_{sys,III}(f)/\mathcal{P}_{sys,I}(f)$. This extends the original definition for equilibrium membrane selectivity[31] to the system's nonequilibrium selectivity, which using eq 12 becomes the ratio between fluxes and bulk concentrations,

$$\alpha_{sys} = \frac{j_{III}/c_{0,III}}{j_I/c_{0,I}} \tag{29}$$

Similarly, using eq 13, the nonequilibrium differential system selectivity, $\alpha^{\Delta}_{sys}(f) \equiv \mathcal{P}^{\Delta}_{sys,III}(f)/\mathcal{P}^{\Delta}_{sys,I}(f)$, leads to the definition of differential selectivity,

$$\alpha^{\Delta}_{sys} = \frac{j'_{III}/c_{0,III}}{j'_I/c_{0,I}} \tag{30}$$

with $j' \equiv dj/df$. The same definition applies to mixture 2 by replacing I with II.

In Figure 7(a) and (b), we show the system selectivity $\alpha_{sys}(f)$ (solid lines) and the differential system selectivity $\alpha^{\Delta}_{sys}(f)$ (dashed lines) for mixtures 1 and 2, respectively. The simulation results for $\alpha_{sys}(f)$, depicted by symbols, are compared with the analytical results based on eq 29 using eq 22. For high $f$, both system and differential system selectivities converge to unity, meaning that there is no selectivity and that all penetrants flow with the limiting flux $j^{\infty}$ derived in eq 24, dictated by the exceedingly high $f$. However, in a small $f$ range in which $j$ is predominantly nonlinear, the selectivity is most sensitive to $f$, which bears a potential fine-tuning of the permselectivity by controlling $f$: Note that we observe a decay of $\alpha^{\Delta}_{sys}(f)$ that goes below unity at around $\beta f = 0.01/\sigma$ in this $f$ range.

## CONCLUSIONS

We have investigated permeability and selectivity for solute transport across a polymer membrane under the action of a generic driving force beyond Fick's law, using penetrant- and polymer-resolved coarse-grained simulations and analytic


https://doi.org/10.1021/acs.macromol.2c00605
Macromolecules XXXX, XXX, XXX−XXX

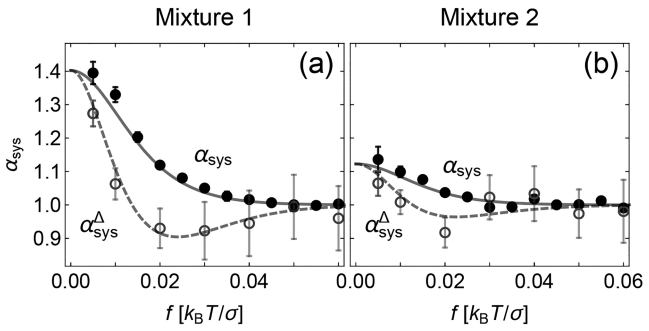


**Figure 7.** System selectivity, $\alpha_{sys}(f)$, in the two-component penetrant mixtures, for (a) mixture 1: $\mathcal{P}^{eq}_{I}/D_0 = 0.13$, $\mathcal{P}^{eq}_{III}/D_0 = 3.3$ and (b) mixture 2: $\mathcal{P}^{eq}_{II}/D_0 = 0.4$, $\mathcal{P}^{eq}_{III}/D_0 = 3.3$. The system selectivities $\alpha_{sys} = \mathcal{P}_{sys,III}(f)/\mathcal{P}_{sys,I}(f)$ and $\alpha_{sys} = \mathcal{P}_{sys,III}(f)/\mathcal{P}_{sys,II}(f)$ (solid lines, see eq 29) are compared with the simulation results (filled circles). The differential system selectivities $\alpha^{\Delta}_{sys}(f) = \mathcal{P}^{\Delta}_{sys,III}(f)/\mathcal{P}^{\Delta}_{sys,I}(f)$ and $\alpha^{\Delta}_{sys}(f) = \mathcal{P}^{\Delta}_{sys,III}(f)/\mathcal{P}^{\Delta}_{sys,II}(f)$ are depicted by the dashed line (see eq 30), compared with the simulation results (empty circles).

solutions from the Smoluchowski "drift−diffusion" theory. We thereby have gone beyond the linear response definition of permeability and extended concepts and definitions of permeability toward nonequilibrium situations. We have presented possible definitions of a force-dependent system permeability and permselectivity, in particular the *differential permeability*, by analytical solutions of the Smoluchowski equation in the steady state, and have verified them by the simulations. As an important consequence, we have demonstrated that in the driven, nonlinear situation the solute selectivity of the system can be tuned and controlled by a small change of the external force. This force control becomes more powerful in low-permeable systems with salient nonlinearity, in which the range of the force is closely related to the system size parameters.

Our study broadens the fundamental understanding of permeability in nonequilibrium transport and provides a foundation for developing theoretical tools to measure and interpret the permeability in driven transport in applications, particularly in strongly driven situations beyond linear response. Owing to the chosen periodic boundary condition in the longitudinal direction, our model, for instance, is feasible for a long tube chamber consisting of periodically repeating membranes that form a multilayer in a dilute solution. For example, one can apply a uniform external electric field to quantify the membrane permeability to dilute ionic solutes using our model (i.e., eqs 18 and 22). Similar electrophoresis, electrodialysis, and sedimentation setups are feasible for our model. However, our framework is not restricted to the periodic boundary condition, to which, in principle, other boundary conditions can be applied. Therefore, applications may further include molecular sieving, translocation, and separation in electrophoresis,[92−94] transport across a membrane controlled by mechanically driven forces,[69] and (electro)dialysis,[8,55,95] to name but a few.

Practical situations may involve more responsive membranes, more strongly interacting solutes, and more strongly coupled hydrodynamics, and thus may require a more sophisticated model based on the presented ideas hereto. It is noteworthy that the distinction between "membrane permeability" and "system permeability" might not be unequivocally possible anymore in nonlinear transport. Hence, the role of system boundary conditions needs to be elucidated in more detail for nonequilibrium situations to serve for better interpretation. Moreover, we believe that our approach will be useful in the study of transport in responsive polymer *feedback-controlled* membranes,[13] i.e., membranes that may deform ("open/close", even switch) locally and return feedback to the transport under the nonequilibrium flow conditions tuned by the inhomogeneous, force-controlled solute density profiles.

## ■ ASSOCIATED CONTENT

### Supporting Information

The Supporting Information is available free of charge at https://pubs.acs.org/doi/10.1021/acs.macromol.2c00605.

Methods; penetrant concentration, longitudinal velocity, and flux; calculation of flux; force-dependent membrane thickness; penetrant concentration profiles for the membrane-only case; and calculation of penetrant concentration profiles (PDF)

## ■ AUTHOR INFORMATION


### Corresponding Authors

**Won Kyu Kim** − *Korea Institute for Advanced Study, Seoul 02455, Republic of Korea;* orcid.org/0000-0002-6286-0925; Email: wonkyukim@kias.re.kr

**Joachim Dzubiella** − *Applied Theoretical Physics−Computational Physics, Physikalisches Institut, Albert-Ludwigs-Universität Freiburg, D-79104 Freiburg, Germany; Cluster of Excellence livMatS @ FIT - Freiburg Center for Interactive Materials and Bioinspired Technologies, Albert-Ludwigs-Universität Freiburg, D-79110 Freiburg, Germany;* orcid.org/0000-0001-6751-1487; Email: joachim.dzubiella@physik.uni-freiburg.de

### Authors

**Sebastian Milster** − *Applied Theoretical Physics−Computational Physics, Physikalisches Institut, Albert-Ludwigs-Universität Freiburg, D-79104 Freiburg, Germany;* orcid.org/0000-0001-6356-7790

**Rafael Roa** − *Departamento de Física Aplicada I, Facultad de Ciencias, Universidad de Málaga, Campus de Teatinos s/n, E-29071 Málaga, Spain;* orcid.org/0000-0003-4439-418X

**Matej Kanduč** − *Jožef Stefan Institute, SI-1000 Ljubljana, Slovenia;* orcid.org/0000-0002-5307-7488

Complete contact information is available at: https://pubs.acs.org/10.1021/acs.macromol.2c00605


### Notes

The authors declare no competing financial interest.

## ■ ACKNOWLEDGMENTS

The authors thank Matthias Ballauff, Michael Bley, Benjamin Rotenberg, Arturo Moncho-Jordá, and Changbong Hyeon for fruitful discussions. This work was supported by the Deutsche Forschungsgemeinschaft via the Research Unit FOR 5099 "Reducing complexity of nonequilibrium systems". W.K.K. acknowledges the support by the KIAS Individual Grants (CG076001 and CG076002) at Korea Institute for Advanced Study and the Center for Advanced Computation at the Korea Institute for Advanced Study for providing computing

resources for this work. M.K. acknowledges the financial support from the Slovenian Research Agency (Contracts P1-0055 and J1-1701).

## REFERENCES

(1) Shasby, D. M.; Shasby, S. S.; Sullivan, J. M.; Peach, M. J. Role of endothelial cell cytoskeleton in control of endothelial permeability. *Circ. Res.* **1982**, *51*, 657−661.
(2) Wingender, J.; Neu, T. R.; Flemming, H.-C. *Microbial Extracellular Polymeric Substances*; Springer, 1999; pp 1−19, DOI: 10.2166/wst.2001.0326.
(3) Hay, E. D. *Cell Biology of Extracellular Matrix*; Springer Science & Business Media, 2013.
(4) Witten, J.; Ribbeck, K.; Khutoryanskiy, V. V.; Wu, L.; Liu, M.; Shan, W.; Zhu, X.; Li, L.; Zhang, Z.; Huang, Y. The particle in the spider's web: transport through biological hydrogels. *Nanoscale* **2017**, *9*, 8080.
(5) Goodrich, C. P.; Brenner, M. P.; Ribbeck, K. Enhanced diffusion by binding to the crosslinks of a polymer gel. *Nat. Commun.* **2018**, *9*, 4348.
(6) Fuhrmann, G. Diffusion and transport of extracellular vesicles. *Nat. Nanotechnol.* **2020**, *15*, 168−169.
(7) Joo, S.; Durang, X.; Lee, O.-c.; Jeon, J.-H. Anomalous diffusion of active brownian particles cross-linked to a networked polymer: langevin dynamics simulation and theory. *Soft Matter* **2020**, *16*, 9188−9201.
(8) Lee, K. P.; Arnot, T. C.; Mattia, D. A Review of reverse osmosis membrane materials for desalination−development to date and future potential. *J. Membr. Sci.* **2011**, *370*, 1−22.
(9) Brazel, C. S.; Peppas, N. A. Mechanisms of solute and drug transport in relaxing, swellable, hydrophilic glassy polymers. *Polymer* **1999**, *40*, 3383−3398.
(10) Stamatialis, D. F.; J.Papenburg, B.; Gironés, M.; Saiful, S.; Bettahalli, S. N. M.; Schmitmeier, S.; Wessling, M. Medical applications of membranes: drug delivery, artificial organs and tissue engineering. *J. Membr. Sci.* **2008**, *308*, 1−34.
(11) Moncho-Jordá, A.; Jódar-Reyes, A. B.; Kanduč, M.; Germán-Bellod, A.; López-Romero, J. M.; Contreras-Cáceres, R.; Sarabia, F.; García-Castro, M.; Pérez-Ramírez, H. A.; Odriozola, G. Scaling laws in the diffusive release of neutral cargo from hollow hydrogel nanoparticles: paclitaxel-loaded poly (4-vinylpyridine). *ACS Nano* **2020**, *14*, 15227−15240.
(12) Carregal-Romero, S.; Buurma, N. J.; Pérez-Juste, J.; Liz-Marzán, L. M.; Hervés, P. Catalysis by Au@PNIPAM nanocomposites: effect of the cross-linking density. *Chem. Mater.* **2010**, *22*, 3051−3059.
(13) Stuart, M. A. C.; Huck, W. T.; Genzer, J.; Müller, M.; Ober, C.; Stamm, M.; Sukhorukov, G. B.; Szleifer, I.; Tsukruk, V. V.; Urban, M.; Winnik, F.; Zauscher, S.; Luzinov, I.; Minko, S. Emerging applications of stimuli-responsive polymer materials. *Nat. Mater.* **2010**, *9*, 101−113.
(14) Lu, Y.; Ballauff, M. Thermosensitive core-shell microgels: from colloidal model systems to nanoreactors. *Prog. Polym. Sci.* **2011**, *36*, 767−792.
(15) Vriezema, D. M.; Comellas Aragonès, M.; Elemans, J. A. A. W.; Cornelissen, J. J. L. M.; Rowan, A. E.; Nolte, R. J. M. Self-assembled nanoreactors. *Chem. Rev.* **2005**, *105*, 1445−1490.
(16) Renggli, K.; Baumann, P.; Langowska, K.; Onaca, O.; Bruns, N.; Meier, W. Selective and responsive nanoreactors. *Adv. Funct. Mater.* **2011**, *21*, 1241−1259.
(17) Tanner, P.; Baumann, P.; Enea, R.; Onaca, O.; Palivan, C.; Meier, W. Polymeric vesicles: from drug carriers to nanoreactors and artificial organelles. *Acc. Chem. Res.* **2011**, *44*, 1039−1049.
(18) Gaitzsch, J.; Huang, X.; Voit, B. Engineering functional polymer capsules toward smart nanoreactors. *Chem. Rev.* **2016**, *116*, 1053−1093.
(19) Guan, Y.; Zhang, Y. PNIPAM microgels for biomedical applications: from dispersed particles to 3D assemblies. *Soft Matter* **2011**, *7*, 6375−6384.
(20) Hervés, P.; Pérez-Lorenzo, M.; Liz-Marzán, L. M.; Dzubiella, J.; Lu, Y.; Ballauff, M. Catalysis by metallic nanoparticles in aqueous solution: model reactions. *Chem. Soc. Rev.* **2012**, *41*, 5577−5587.
(21) Wu, S.; Dzubiella, J.; Kaiser, J.; Drechsler, M.; Guo, X.; Ballauff, M.; Lu, Y. Thermosensitive Au-PNIPA yolk-shell nanoparticles with tunable selectivity for catalysis. *Angew. Chem., Int. Ed.* **2012**, *51*, 2229−2233.
(22) Prieto, G.; Tüysüz, H.; Duyckaerts, N.; Knossalla, J.; Wang, G.-H.; Schüth, F. Hollow nano-and microstructures as catalysts. *Chem. Rev.* **2016**, *116*, 14056−14119.
(23) Petrosko, S. H.; Johnson, R.; White, H.; Mirkin, C. A. Nanoreactors: small spaces, big implications in chemistry. *J. Am. Chem. Soc.* **2016**, *138*, 7443−7445.
(24) Jia, H.; Roa, R.; Angioletti-Uberti, S.; Henzler, K.; Ott, A.; Lin, X.; Möser, J.; Kochovski, Z.; Schnegg, A.; Dzubiella, J.; Ballauff, M.; Lu, Y. Thermosensitive Cu2O-PNIPAM core-shell nanoreactors with tunable photocatalytic activity. *J. Mater. Chem. A* **2016**, *4*, 9677−9684.
(25) Robeson, L. M. Correlation of separation factor versus permeability for polymeric membranes. *J. Membr. Sci.* **1991**, *62*, 165−185.
(26) Pandey, P.; Chauhan, R. Membranes for gas separation. *Prog. Polym. Sci.* **2001**, *26*, 853−893.
(27) Atci, E.; Erucar, I.; Keskin, S. Adsorption and transport of ch4, co2, h2 mixtures in a bio-mof material from molecular simulations. *J. Phys. Chem. C* **2011**, *115*, 6833−6840.
(28) Falk, K.; Coasne, B.; Pellenq, R.; Ulm, F.-J.; Bocquet, L. Subcontinuum mass transport of condensed hydrocarbons in nanoporous media. *Nat. Commun.* **2015**, *6*, 6949.
(29) Obliger, A.; Pellenq, R.; Ulm, F.-J.; Coasne, B. Free volume theory of hydrocarbon mixture transport in nanoporous materials. *J. Phys. Chem. Lett.* **2016**, *7*, 3712−3717.
(30) Freeman, B. D. Basis of permeability/selectivity tradeoff relations in polymeric gas separation membranes. *Macromolecules* **1999**, *32*, 375−380.
(31) Park, H. B.; Kamcev, J.; Robeson, L. M.; Elimelech, M.; Freeman, B. D. Maximizing the right stuff: the trade-off between membrane permeability and selectivity. *Science* **2017**, *356*, 1137.
(32) Bilchak, C. R.; Jhalaria, M.; Huang, Y.; Abbas, Z.; Midya, J.; Benedetti, F. M.; Parisi, D.; Egger, W.; Dickmann, M.; Minelli, M.; Doghieri, F.; Nikoubashman, A.; Durning, C. J.; Vlassopoulos, D.; Jestin, J.; Smith, Z. P.; Benicewicz, B. C.; Rubinstein, M.; Leibler, L.; Kumar, S. K. Tuning selectivities in gas separation membranes based on polymer-grafted nanoparticles. *ACS Nano* **2020**, *14*, 17174−17183.
(33) He, G.; Mi, Y.; Yue, P. L.; Chen, G. Theoretical study on concentration polarization in gas separation membrane processes. *J. Membr. Sci.* **1999**, *153*, 243−258.
(34) Pan, C. Y.; Habgood, H. W. An analysis of the single-stage gaseous permeation process. *Ind. Eng. Chem., Fundam.* **1974**, *13*, 323−331.
(35) Shannon, M. A.; Bohn, P. W.; Elimelech, M.; Georgiadis, J. G.; Mariñas, B. J.; Mayes, A. M. Science and technology for water purification in the coming decades. *Nature* **2008**, *452*, 301−310.
(36) Geise, G. M.; Lee, H.-S.; Miller, D. J.; Freeman, B. D.; McGrath, J. E.; Paul, D. R. Water purification by membranes: the role of polymer science. *J. Polym. Sci., Part B* **2010**, *48*, 1685−1718.
(37) Geise, G. M.; Park, H. B.; Sagle, A. C.; Freeman, B. D.; McGrath, J. E. Water permeability and water/salt selectivity tradeoff in polymers for desalination. *J. Membr. Sci.* **2011**, *369*, 130−138.
(38) Menne, D.; Pitsch, F.; Wong, J. E.; Pich, A.; Wessling, M. Temperature-modulated water filtration using microgel-functionalized hollow-fiber membranes. *Angew. Chem., Int. Ed.* **2014**, *53*, 5706−5710.
(39) Tansel, B.; Sager, J.; Rector, T.; Garland, J.; F.Strayer, R.; Levine, L.; Robert, M.; Hummerick, M.; Bauer, J. Significance of hydrated radius and hydration shells on ionic permeability during nanofiltration in dead end and cross flow modes. *Sep. Purif. Technol.* **2006**, *51*, 40−47.


https://doi.org/10.1021/acs.macromol.2c00605
*Macromolecules* XXXX, XXX, XXX−XXX

(40) Tan, Z.; Chen, S.; Peng, X.; Zhang, L.; Gao, C. Polyamide membranes with nanoscale turing structures for water purification. *Science* **2018**, *360*, 518−521.
(41) Hyk, W.; Kitka, K. Water purification using sponge like behaviour of poly (N-isopropylacrylamide) ferrogels. studies on silver removal from water samples. *J. Environ. Chem. Eng.* **2018**, *6*, 6108−6117.
(42) Lu, X.; Feng, X.; Yang, Y.; Jiang, J.; Cheng, W.; Liu, C.; Gopinadhan, M.; Osuji, C. O.; Ma, J.; Elimelech, M. Tuning the permselectivity of polymeric desalination membranes via control of polymer crystallite size. *Nat. Commun.* **2019**, *10*, 1−7.
(43) Graham, T. On the absorption and dialytic separation of gases by colloid septa. *Philos. Mag.* **1866**, *32*, 401−420.
(44) Missner, A.; Pohl, P. 110 years of the meyer−overton rule: predicting membrane permeability of gases and other small compounds. *ChemPhysChem* **2009**, *10*, 1405−1414.
(45) Finkelstein, A. *Water Movement through Lipid Bilayers, Pores, and Plasma Membranes: Theory and Reality*; John Wiley & Sons: New York, 1987; Vol. *4*, DOI: 10.1086/415748.
(46) Al-Awqati, Q. One hundred years of membrane permeability: does Overton still rule? *Nat. Cell Biol.* **1999**, *1*, No. E201.
(47) Venable, R. M.; Krämer, A.; Pastor, R. W. Molecular dynamics simulations of membrane permeability. *Chem. Rev.* **2019**, *119*, 5954−5997.
(48) Wolde-Kidan, A.; Herrmann, A.; Prause, A.; Gradzielski, M.; Haag, R.; Block, S.; Netz, R. R. Particle diffusivity and free-energy profiles in hydrogels from time-resolved penetration data. *Biophys. J.* **2021**, *120*, 463−475.
(49) Gehrke, S.; Fisher, J.; Palasis, M.; Lund, M. E. Factors determining hydrogel permeability. *Ann. N.Y. Acad. Sci.* **1997**, *831*, 179−207.
(50) Nelson, P. *Biological Physics*; WH Freeman: New York, 2004.
(51) Yasuda, H.; Peterlin, A.; Colton, C.; Smith, K.; Merrill, E. Permeability of solutes through hydrated polymer membranes. part iii. theoretical background for the selectivity of dialysis membranes. *Die Makromol. Chem.* **1969**, *126*, 177−186.
(52) Diamond, J. M.; Katz, Y. Interpretation of nonelectrolyte partition coefficients between dimyristoyl lecithin and water. *J. Membr. Biol.* **1974**, *17*, 121−154.
(53) Paul, D. R. The solution-diffusion model for swollen membranes. *Sep. Purif. Methods* **1976**, *5*, 33−50.
(54) Wijmans, J. G.; Baker, R. W. The solution-diffusion model: a review. *J. Membr. Sci.* **1995**, *107*, 1−21.
(55) Mason, E. A.; Lonsdale, H. K. Statistical-mechanical theory of membrane transport. *J. Membr. Sci.* **1990**, *51*, 1−81.
(56) Palasis, M.; Gehrke, S. H. Permeability of responsive poly (n-isopropylacrylamide) gel to solutes. *J. Controlled Release* **1992**, *18*, 1−11.
(57) George, S. C.; Thomas, S. Transport phenomena through polymeric systems. *Prog. Polym. Sci.* **2001**, *26*, 985−1017.
(58) Ulbricht, M. Advanced functional polymer membranes. *Polymer* **2006**, *47*, 2217−2262.
(59) Baker, R. W.; Low, B. T. Gas separation membrane materials: a perspective. *Macromolecules* **2014**, *47*, 6999−7013.
(60) Smoluchowski, M. V. Über Brownsche Molekularbewegung unter Einwirkung äußerer Kräfte und deren Zusammenhang mit der verallgemeinerten Diffusionsgleichung. *Ann. Physik* **1915**, *48*, 1103.
(61) Fokker, A. D. Die mittlere Energie rotierender elektrischer Dipole im Strahlungsfeld. *Ann. Physik* **1914**, *348*, 810.
(62) Planck, M. Über einen Satz der statistischen Dynamik und seine Erweiterung in der Quantentheorie. Sitzber. K. *Preuss. Aka.* **1917**, 324.
(63) Risken, H. *The Fokker-Planck Equation*; Springer, 1996.
(64) Doi, M.; Edwards, S. F. *The Theory of Polymer Dynamics*; Oxford University Press, 1988.
(65) Dhont, J. K. G. *An Introduction to Dynamics of Colloids*; Elsevier Science B.V., 1996.
(66) Paul, D. R. Reformulation of the solution-diffusion theory of reverse osmosis. *J. Membr. Sci.* **2004**, *241*, 371−386.
(67) Marrink, S.-J.; Berendsen, H. J. C. Simulation of water transport through a lipid membrane. *J. Phys. Chem.* **1994**, *98*, 4155−4168.
(68) Hwang, S.-T. Fundamentals of membrane transport. *Korean J. Chem. Eng.* **2011**, *28*, 1−15.
(69) Alberts, B.; Johnson, A.; Lewis, J.; Raff, M.; Roberts, K.; Walter, P. *Molecular Biology of the Cell*, 4th ed.; Garland Science, 2002.
(70) Wang, L.; Cao, T.; Dykstra, J. E.; Porada, S.; Biesheuvel, P. M.; Elimelech, M. Salt and water transport in reverse osmosis membranes: beyond the solution-diffusion model. *Environ. Sci. Technol.* **2021**, *55*, 16665−16675.
(71) Kim, W. K.; Moncho-Jordá, A.; Roa, R.; Kanduč, M.; Dzubiella, J. Cosolute partitioning in polymer networks: effects of flexibility and volume transitions. *Macromolecules* **2017**, *50*, 6227−6237.
(72) Kim, W. K.; Kanduč, M.; Roa, R.; Dzubiella, J. Tuning the permeability of dense membranes by shaping nanoscale potentials. *Phys. Rev. Lett.* **2019**, *122*, 108001.
(73) Kim, W. K.; Chudoba, R.; Milster, S.; Roa, R.; Kanduč, M.; Dzubiella, J. Tuning the selective permeability of polydisperse polymer networks. *Soft Matter* **2020**, *16*, 8144−8154.
(74) Milster, S.; Kim, W. K.; Kanduč, M.; Dzubiella, J. Tuning the permeability of regular polymeric networks by the cross-link ratio. *J. Chem. Phys.* **2021**, *154*, 154902.
(75) Kanduč, M.; Kim, W. K.; Roa, R.; Dzubiella, J. Modeling of stimuli-responsive nanoreactors: rational rate control towards the design of colloidal enzymes. *Mol. Syst. Des. Eng.* **2020**, *5*, 602−619.
(76) Kanduč, M.; Kim, W. K.; Roa, R.; Dzubiella, J. How the shape and chemistry of molecular penetrants control responsive hydrogel permeability. *ACS Nano* **2021**, *15*, 614−624.
(77) Roa, R.; Kim, W. K.; Kanduč, M.; Dzubiella, J.; Angioletti-Uberti, S. Catalyzed bimolecular reactions in responsive nanoreactors. *ACS Catal.* **2017**, *7*, 5604−5611.
(78) Heyda, J.; Muzdalo, A.; Dzubiella, J. Rationalizing polymer swelling and collapse under attractive cosolvent conditions. *Macromolecules* **2013**, *46*, 1231−1238.
(79) Stratonovich, R. L. *Non-Linear Transformations of Stochastic Processes*; Elsevier, 1965; pp 269−282.
(80) Dagdug, L.; Berezhkovskii, A. M.; Makhnovskii, Y. A.; Zitserman, V. Y.; Bezrukov, S. M. Force-dependent mobility and entropic rectification in tubes of periodically varying geometry. *J. Chem. Phys.* **2012**, *136*, 214110.
(81) Esaki, L.; Tsu, R. Superlattice and negative differential conductivity in semiconductors. *IBM J. Res. Dev.* **1970**, *14*, 61−65.
(82) Lei, X. L.; Horing, N. J. M.; Cui, H. L. Theory of negative differential conductivity in a superlattice miniband. *Phys. Rev. Lett.* **1991**, *66*, 3277.
(83) Labouvie, R.; Santra, B.; Heun, S.; Wimberger, S.; Ott, H. Negative differential conductivity in an interacting quantum gas. *Phys. Rev. Lett.* **2015**, *115*, 050601.
(84) Albers, R. Biochemical aspects of active transport. *Annu. Rev. Biochem.* **1967**, *36*, 727−756.
(85) Baranowski, B. Non-equilibrium thermodynamics as applied to membrane transport. *J. Membr. Sci.* **1991**, *57*, 119−159.
(86) Tang, J.; Du, N.; Doyle, P. S. Compression and self-entanglement of single DNA molecules under uniform electric field. *Proc. Natl. Acad. Sci. U.S.A.* **2011**, *108*, 16153−16158.
(87) Costantini, G.; Marchesoni, F. Threshold diffusion in a tilted washboard potential. *Europhys. Lett.* **1999**, *48*, 491.
(88) Reimann, P.; Van den Broeck, C.; Linke, H.; Hänggi, P.; Rubi, J. M.; Pérez-Madrid, A. Giant acceleration of free diffusion by use of tilted periodic potentials. *Phys. Rev. Lett.* **2001**, *87*, 010602.
(89) Lindner, B.; Kostur, M.; Schimansky-Geier, L. Optimal diffusive transport in a tilted periodic potential. *Fluct. Noise Lett.* **2001**, *1*, R25−R39.
(90) Burada, P. S.; Hänggi, P.; Marchesoni, F.; Schmid, G.; Talkner, P. Diffusion in confined geometries. *ChemPhysChem* **2009**, *10*, 45−54.
(91) Hänggi, P.; Marchesoni, F. Artificial Brownian motors: controlling transport on the nanoscale. *Rev. Mod. Phys.* **2009**, *81*, 387.
(92) Hjertén, S. Molecular-sieve" electrophoresis in cross-linked polyacrylamide gels. *J. Chromatogr. A* **1963**, *11*, 66−70.


https://doi.org/10.1021/acs.macromol.2c00605
*Macromolecules* XXXX, XXX, XXX−XXX

(93) Ajdari, A.; Prost, J. Free-flow electrophoresis with trapping by a transverse inhomogeneous field. *Proc. Natl. Acad. Sci. U.S.A.* **1991**, *88*, 4468−4471.
(94) Nkodo, A. E.; Garnier, J. M.; Tinland, B.; Ren, H.; Desruisseaux, C.; McCormick, L. C.; Drouin, G.; Slater, G. W. Diffusion coefficient of dna molecules during free solution electrophoresis. *Electrophoresis* **2001**, *22*, 2424−2432.
(95) Soltanieh, M.; Gill, W. N. Review of reverse osmosis membranes and transport models. *Chem. Eng. Commun.* **1981**, *12*, 279−363.


https://doi.org/10.1021/acs.macromol.2c00605
*Macromolecules* XXXX, XXX, XXX−XXX